

Robot-assisted Mechanical Scanning and Co-registration of Magnetic Resonance Imaging and Light-Induced Fluorescence

Ahmet E. Sonmez, William M. Spees, Alpay Özcan, Zhigang Deng, Andrew G. Webb and Nikolaos V. Tsekos

Abstract—Robotic manipulators offer some unique opportunities to address research and clinical needs. Among those is the potential use of a robotic manipulator to mechanically scan the tissue of interest with biosensors that have limited tissue penetration. In such cases, the robot can serve a dual role. First, it can perform spatial scanning with the biosensor along a pre-selected path inside the tissue. Second, it can function as the mechanical link to spatially co-register the data collected with the biosensor and the images of a guidance modality. Herein, we describe a robotic system to mechanically scan with a light-induced fluorescence (LIF) sensor and co-register LIF data to the guiding modality of MRI. Specifically, a custom-built MR-compatible endoscope was integrated onto the end-effector of an MR-compatible manipulator to collect MRI-guided LIF 1D scans. A miniature radiofrequency (RF) coil attached onto the end-effector was used as a fiducial marker for co-registering LIF and MRI. This mechanically scanning system was investigated on two compartment phantoms, each with different optical agents. Those studies demonstrated “robot-assisted” multi-modality co-registration, i.e. the spatial distribution of the LIF signals matched with the MR guiding images. The system can incorporate additional sensors for collecting complementary biochemical information.

I. INTRODUCTION

An overgrowing body of literature supports the notion that experimental understanding and clinical diagnosis of the disease, often requires the collection of complementary information available with multimodality imaging (e.g. in the case of breast [1, 2] or prostate [3] cancer). A critical area in modern medicine is the

Manuscript received January 31, 2012. This work was supported by the National Science Foundation (NSF) award CNS-0932272. All opinions, findings, conclusions or recommendations expressed in this work are those of the authors and do not necessarily reflect the views of our sponsors.

Nikolaos V. Tsekos and Ahmet E. Sonmez are with the Medical Robotics Laboratory, Department of Computer Science at University of Houston, Houston, TX, USA (phone: 713-743-3350; fax: 713-743-3335; (e-mail: ntsekos@cs.uh.edu, asonmez@uh.edu).

William M. Spees is with the Biomedical Magnetic Resonance Laboratory, Washington University, St. Louis, MO, USA (e-mail: spees@wuchem.wustl.edu).

Alpay Özcan is with the Arlington Innovation Center, Virginia Polytechnic Institute and State University, Arlington, VA, USA (email: alpay@vt.edu).

Zhigang Deng is with Computer Graphics & Interactive Media Lab and Computer Science Department, at University of Houston, Houston, TX 77004, USA (email: zdeng@cs.uh.edu).

Andrew G. Webb is with the Department of Radiology, Leiden University Medical Center, Leiden, Netherlands, The Netherlands (email: a.webb@lumc.nl).

introduction and advancement of modalities that assess the features of lesions in vivo at the molecular and/or cellular level [4]. Examples of such modalities are LIF, confocal microscopy (CoM) and optical coherence tomography (OCT).

While such modalities offer unique complementary information and new opportunities in research and clinical diagnosis (e.g. [5]), they also face a critical impediment: limited tissue penetration ($\sim 1-3$ mm for optical methods, depending on wavelength) [6]. For this reason, herein, we will refer to those modalities as “Limited field-of-view (Limited-FOV)”. To address this, trans-needle and trans-catheter approaches are used. Secondary to this limitation is also the necessity to use another modality, i.e. a Wide-FOV one, to locate the targeted lesion and guide the placement of the Limited-FOV sensor. Examples of such Wide-FOV are Magnetic Resonance Imaging (MRI)[2] or ultrasound [7]. Moreover, practical use of the Limited-FOV sensors also requires scanning to assess different types of tissue (e.g. healthy vs. lesion). Finally, it is also important to co-register the Limited- and Wide-FOV data.

MRI compatible robotic methodology can address the above mentioned challenges (e.g. for MR compatible robotics [8]). Specifically, if an appropriately designed and controlled manipulator is the carrier of the Limited-FOV sensors, then (1) spatial scanning of the area of interest can be performed by stepwise mechanical translation of the Limited-FOV sensor(s), and (2) co-registration of different modalities (Wide- and Limited-FOV) can be achieved without using computationally expensive methods for image-based registrations [9].

This work presents a new system for robot-assisted multi-modality MR/optical scanning that integrates MRI and LIF. It is based on our previous work [10] that used a robotic manipulator to mechanically scan a miniature RF coil to collect highly localized proton (^1H) MR spectra. In that previous work the Limited FOV modality was proton (^1H) MR spectroscopy. Herein, the Limited FOV modality is LIF and in the clinical scenario it will be used to assess the content of endogenous or exogenous (i.e. contrast agents) fluorophores in the tissue (that are markers of the disease) [11]. MRI is the Wide-FOV modality and used for: (1) planning the mechanical scan of the LIF sensors, and (2) registering the LIF sensor.

The major contributions and novelties of this work are (1) a custom-made MR-compatible dual sensor MR/LIF probe (the LIF sensor implemented with two optical fibers for reception and one for light emission and the MR sensor with a 1.0 mm wide miniature RF coil), (2) experimental demonstration of robot-assisted combined MR imaging and LIF, (3) a control scheme for the image-based automatic scanning that synchronizes robot motion and scanning. With this implementation, we collected LIF spectra along the axis of the manipulator on phantoms and generated one-dimensional (1D) LIF spectra that were co-registered to the guiding MR scout images.

II. METHODS

A. Principles of Robot-Assisted Biosensing

The described system for performing multimodality imaging by using a robotic manipulator as a “mechanical” link between the different modalities based on the following three principles of operation: (a) *Scanning*: the robotic manipulator carries one or more Limited-FOV sensor(s), and mechanically scans an area of interest. In this work, the manipulator carries an endoscopic LIF sensor for optical spectroscopy. (b) *Guidance*: A Wide-FOV modality is used for scout imaging, selection of the area of interest and image-based guidance of robot mechanical scans with the Limited-FOV sensor(s). In this work we use scout MRI to set the areas for scanning. (c) *Co-registration*: The robotic manipulator is registered to the Wide-FOV modality coordinate system; encoder reading of the manipulator is then used to spatially register the exact areas where the Limited-FOV collects data. In this work, the resident coordinate system of the MR scanner is used for registering the manipulator using a miniature RF coil as a fiducial marker.

B. Overview of the System:

Fig. 1 shows the architecture of the MRI/LIF robot assisted biosensing system that is composed of several interconnected components. For MR compatibility, the hardware components are organized in two groups: (a) those residing in the MR console room and away from the MR scanner (the PC, controller box, optical spectrometer as shown in the fig. 2) and (b) those inside the MR scanner were fully MR compatible and MR safe, (the MR compatible manipulator (fig. 3) and the probe (fig. 4).) These two groups are connected via optical fibers and shielded coaxial wires.

The MR scanner provided two types of data: (1) Scout images of the phantom with a volume coil for planning the position and area to be mechanically scanned and (2) a scout image with miniature surface RF coil for co-registration of manipulator, thus LIF to the MR coordinate system. This image provided the reference position for multimodal co-registration with the method we used in our former work [10].

An in house made electronic component, the “control box”, was used to manage movement of the probe, and automatically synchronize MR and LIF data collection.

The optical spectrometer (USB 2000+, Ocean Optics, Dunedin, FL) was triggered from the control box to collect the optical spectra while the robot was idle after moving the MR/LIF probe to the designated points. The light source used was LED (Light Emitting Diode) with peak wavelength at 450 nm (LED 470 filtered at 450nm, Ocean Optics, Dunedin, FL).

An MR-compatible manipulator was developed for trans-needle mechanical spatial scanning of the in-house developed MR/LIF probe (described in section II.C). The manipulator was actuated with a motor operating based on the piezoelectric phenomenon (N-310 NEXACT Piezo-Walk motor, PI, Karlsruhe, Germany). The Piezo-Walk motor was driven with a dedicated motor driver and controller (E-861

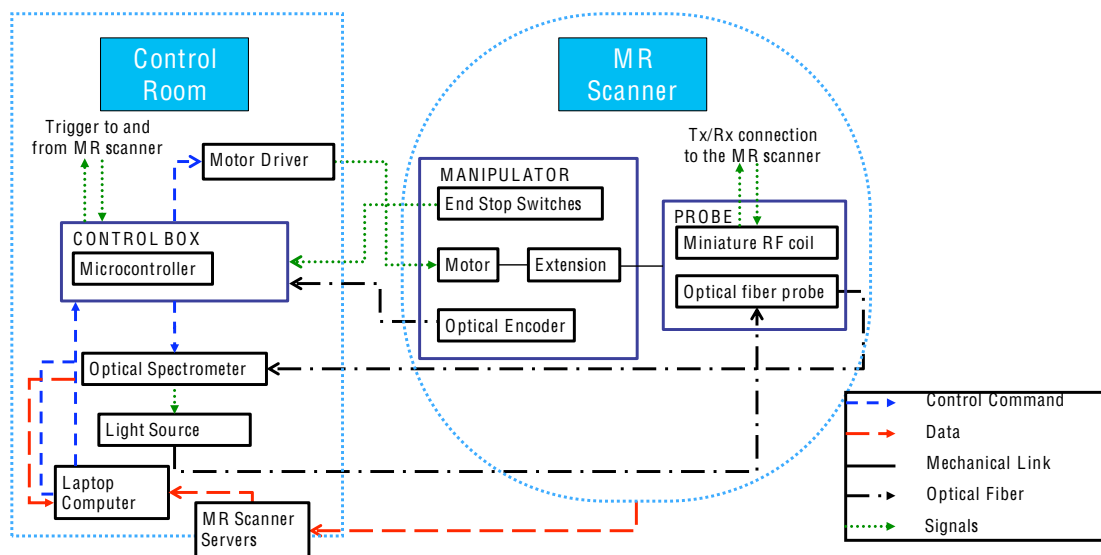


Fig. 1. Architecture of the MRI/LIF robot assisted biosensing system.

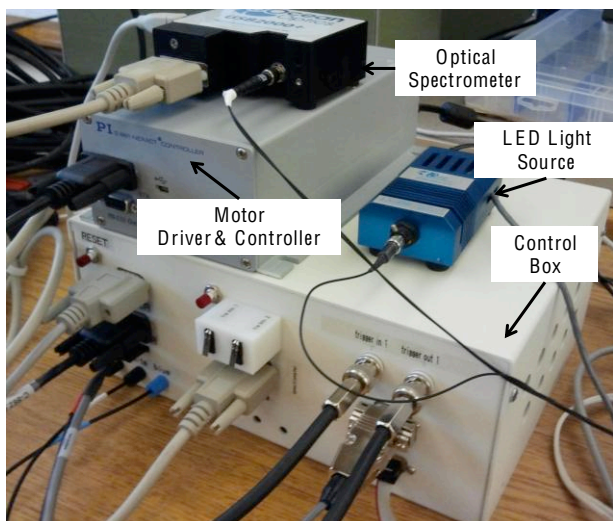


Fig. 2. Hardware components residing in the control room (laptop PC is not shown here).

NEXACT Controller, PI, Karlsruhe, Germany). In our implementation this controller was only used to drive the motor with the control signals generated by the controller box i.e. by sending control commands through a serial port.

C. Dual MR/LIF Probe

We designed and constructed a dual MR/LIF probe. To construct this probe we used four bore, 1.6 mm diameter quartz tubing that aligned the optical fibers of the LIF probe and carried the coaxial cable of the miniature RF coil.

The optical fibers (core/cladding/buffer = 200/220/245 microns, 0.22NA, plastic) were terminated with 0.5 mm leg size prisms (P-788474-S-RTA002, Bern Optics, Westfield, MA) (fig. 4(b)) to direct the light beam orthogonal to the

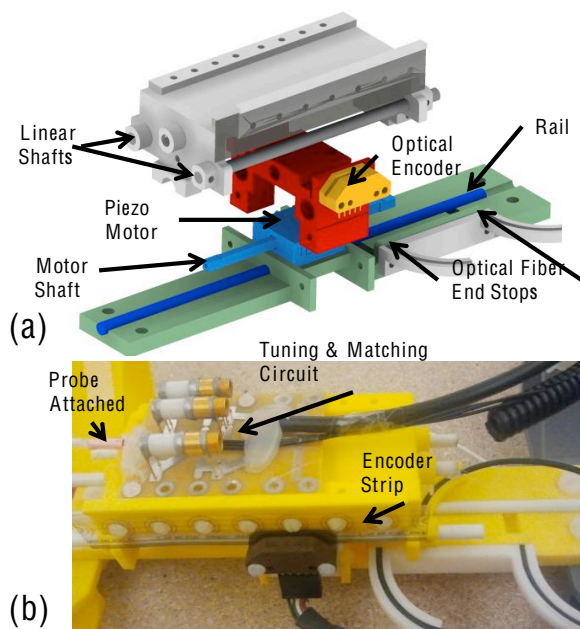


Fig. 3. (a) 3D design of the manipulator (b) Picture of assembled manipulator. Tuning&Matching circuit is attached on the manipulator.

axis of the needle for “side viewing”. As illustrated in fig. 4, one optical fiber (S) was used for transmitting light from the LED light source for excitation, and two optical fibers (R1 and R2) for receiving light from the investigated area. The two receiving fibers were then combined (in an optical coupler) and fed to the optical spectrometer. The MR probe was a miniature RF coil constructed out of 313 microns outside diameter (OD) coaxial cable (50MCX-21, Temp-Flex, South Grafton, MA). The stripped distal end of the center conductor of the coaxial cable was whirled to form a 1 mm diameter loop. The other end of the coaxial cable was connected to its tuning & matching circuit. This balanced tuning and matching circuit was constructed using variable non-magnetic capacitors (Johanson Manufacturing Co, Boonton, NJ) for fine tuning and matching at the proton Larmor frequency of 201.5 MHz (the operating frequency of the employed 4.7 Tesla MR scanner). The miniature RF coil and the above-mentioned quartz tubing were attached using optical adhesive (Norland 72, Cranbury, NJ). Since the prisms of the optical probe were coated with a thin film of aluminum, to avoid any distortion of the local magnetic field due to eddy currents or other artifacts due to impurities in the coating, the miniature coil was placed 1 cm away from the optical prisms (fig. 4(a)).

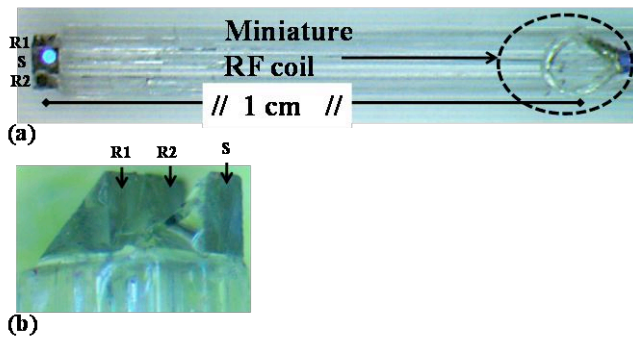


Fig. 4. MR/LIF probe, total OD is 1.9 mm . (a) Light is illuminated from source fiber Locations of two Receiving fibers (R1,R2) and one source (S) fiber are marked. (b) Rotated view of the tip of the probe, 0.5mm leg size prisms are seen in the picture.

D. Design and Prototyping

Fig. 3(a) shows the part of the manipulator. The design includes two linear shafts and one rail shaft in addition to motor shaft for stability and rigidity of the translating component. The device was built with acrylonitrile butadiene styrene (ABS P400, a non-magnetic and non-conductive MR compatible material) using a rapid prototyping machine (model: Prodigy Plus, Stratasys, Eden Prairie, MN). Individually built parts were then assembled to the final form (Fig 3(b)).

E. Control

A microcontroller (MC9S12DG256, 16-bit microcontroller, Freescale, Austin, Texas) based control box was designed to control the system in real time. The control box was receiving experimental parameters from computer, and transmitting control commands with the motor driver and controller through RS232 connections. The MR scanner and

optical spectrometer were also synchronized with the control box to perform an acquisition scheme.

An optical encoder (EM-1, US Digital, Vancouver, WA) and in house built optical end stops [10] were used for closed loop control. A Proportional Derivative (PD) control loop feedback mechanism was used to control the speed of the motor motion, between each step of data acquisition. The speed of the Piezo-Walk motor can be adjusted either by changing its step size, which is tuned by voltage parameter, or by changing its steps per second, which is tuned by frequency parameter. Here we used PD control to adjust the frequency parameter of the Piezo-Walk motor.

F. Simulations

Simulations were initially performed to assess the spatial sensitivity profile of the Limited-FOV sensor, i.e. optical fibers. This was necessary to determine optimum scanning resolution depending on the profile of Limited-FOV sensor.

To model the sensitive area of fluorescence detection we modified and used a three-dimensional, weighted-photon Monte Carlo simulation code [12], which is traditionally used to simulate photon transportation in and interaction with turbid media. We made two in-house modifications on this code: (1) to simulate the fluorescence according to the model and the equations derived in [13], and (2) added the capability to be able to excite the medium using a circular source instead of a point source. During the simulation, if the photon experiences fluorescence (which means the wavelength has been changed), the location where the fluorescence occurred is temporarily recorded then if the same photon reaches to the receiving probe, the counter is incremented by one for that specific voxel. Three dimensional data, mapping the simulation volume is saved at the end of the simulation. This 3D data delineated the fluorescence receiving profile.

Simulations were performed assuming a uniform medium (i.e., single layer) with the parameters of human epithelial tissue at 460 nm reported and used in [13]. These parameters were: Refractive index $n=1.37$, absorption coefficient $\mu_a = 10.871 \text{ cm}^{-1}$, scattering coefficient $\mu_s = 75.0 \text{ cm}^{-1}$, anisotropy $g = 0.94$ and a yield $y = 1$. A total of 2 billion photons were emitted. The simulation was conducted in a $200 \times 400 \times 400$ volumetric matrix with a grid size of 5 microns. Tissue properties of $\mu_a = 9.00 \text{ cm}^{-1}$, $\mu_s = 70.8 \text{ cm}^{-1}$, and $g = 0.94$ is used for the photons travelling in the tissue after experiencing the fluorescence, assuming the new photon wavelength to be 520 nm [13]. Only one receiving optical fiber is used for performing simulations, and we benefit from symmetry for the further analysis with two receiving fibers in section III. The source fiber is located at the center and the receiving fiber (R2) is located 400 microns away from the center. 250 microns diameter is used for both optical fibers.

Fig. 5 is a simulation result of a 5 micron slice along the centers of optical fibers, showing the sensitivity profile of the receiving probe R2. This result is further analyzed to determine the scanning resolution in section III.

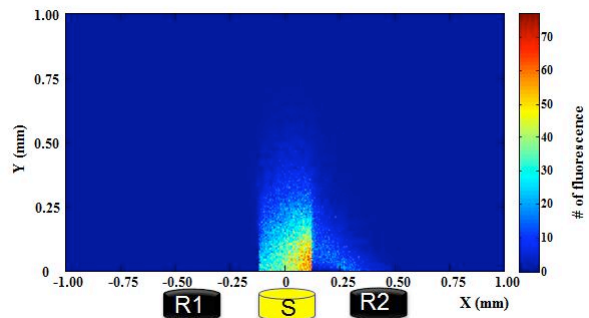


Fig. 5. Sensitivity profile of the receiving probe R2. The relative positions of the receiving fibers (R1, R2) and the source fiber (S) are also shown .

G. Experimental Studies

The MRI/LIF system was tested on a Varian/Agilent DirectDrive™ MR spectrometer/imager system (Agilent Technologies, Santa Clara, CA). Studies were performed to assess whether the existence of motor in the MR scanner introduce noise to the MR Images. In these studies we used a 6.5 % gelatin/water phantom with a volume RF coil around it. Then, we collected scout MRI (30 repetitions), for two cases: (1) motor does not exist. (2) Motor exists in the scanner but idle, as in the case of guiding MR images for the phantom studies are collected (manipulator at its exact position, with the motor 55 cm away from the isocenter of the magnet). From these data, we extracted the signal-to-noise ratio (SNR).

Studies were performed using two-compartment rectangular phantoms (23.5 mm x 23.5 mm x 15 mm inside dimensions). All compartments were filled by gelatin phantoms. First compartment (comp1) was filled with water based gelatin phantom comprising fluorescein (518-47-8, Acros Organics, Morris Plains, NJ) as a fluorophore. This phantom was prepared by first adding 6.5 gr. of gelatin (~200 Bloom) onto 100 ml warm water then mixing until gelatin dissolves. We also added milk (8.5ml, whole milk), fluorescein (3ml, 7.98mM) and EDTA (0.01M, 1ml, Sigma Aldrich, St. Louis, MO). After dissolving all the components we poured it into the phantom mold and kept in the refrigerator until it becomes solid. For the second compartment (comp2) we used Aloe Vera Juice (99.8% Aloe Vera, CVS/pharmacy) instead of water. We also added rhodamine-B (2ml, 6×10^{-4} mM) in addition to the fluorescein. This way we aimed to observe the transition of the optical signal while the optical probe was scanning through the compartments. By using Aloe Vera in the second compartment we obtained a contrast in the MR images, among the comp1 and comp2.

Comp1 and comp2 were stacked together, and an optically clear tube (a 2.5 mm OD NMR tube) was inserted through the centers of the phantom compartments as an endoscopic access cannula. Phantoms were placed inside a volume RF coil (73 mm ID) for wide-FOV imaging.

Initially, scout images were collected with the volumetric RF coil (TR/TE/ α = 30ms/5ms/20°; slice thickness = 2 mm; acquisition matrix 128x128; pixel size 0.039 mm x 0.039 mm) for planning. And the device was registered to the MR scanner using the miniature RF coil as a fiducial marker [10]. Using the GUI graphical tools an exact scanning protocol was selected (region and steps/resolution). The manipulator advanced the probe along the path of scanning and stopped in steps of 0.5 mm, where an LIF spectrum was collected with 5s of integration. The control software with the triggering scheme allowed automation of the procedure.

III. RESULTS

MR-compatibility studies demonstrated that when the manipulator was present in the scanner but idle (i.e. at the condition of optical or MR data collection), there were no significant effects on image. Specifically signal to noise ratio (SNR) values of MR images (mean SNR \pm std of SNR for a data set of 30) are measured as in the table below.

TABLE I

SNR FOR MR IMAGES WITH AND WITHOUT MOTOR

Motor Status	SNR
No motor	76.53 \pm 2.43
Powered (idle)	73.34 \pm 2.80

Data were collected with motor idle (powered but not running).

We integrated the result of simulation (with two receiving probes) volume along the X axis (along the center of optical fibers shown in fig. 6 (a)) and along the Z axis (scanning axis, shown in fig. 6(b)). By selecting 0.5 mm scanning resolution, each LIF is performed more than three standard deviations (of profile in Z axis) away (more than 99.73% assuming normal distribution) from the previous and next LIF (-0.25 mm to 0.25 mm has 98.07% of the total profile). Although this assumption is not perfect at the borders (explained in section IV) simulations can help to determine, optimum scanning resolution, when time is considered, taking into consideration that each LIF scan took 5s.

Fig. 7(b) shows a stack plot of optical spectra collected every 0.5 mm along the Z axis of the scanner. The

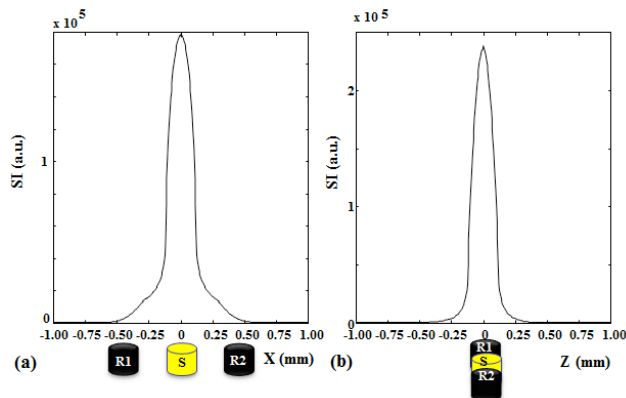


Fig. 6. Integral of intensities along the (a) X axis and (b) Z axis. Z axis was the scanning direction with the LIF probe. Receiving (R1, R2) and Source fiber (S) locations are also shown in the figures.

transition between the compartments is apparent at $Z = -0.15$ cm. This is manifested with the emergence of the rhodamine-B in the comp2 in addition to fluorescein in the comp1 and comp2. In comp1, fluorescein gave rise to fluorescence emission spectra with a characteristic emission peak at 520 nm. In comp2, rhodamine-B absorbed light at 550 nm that is emitted by fluorescein, and emitted fluorescence with a characteristic peak at 573 nm. As a result, the emission spectrum of comp2 exhibited emission peak at 520 nm and 573 nm, and a characteristic absorption dip at 550 nm.

Transition boundary, the start ($Z = -1.65$ cm) and end points ($Z = 1.35$ cm) of the phantom, with respect to the Z axis of the MR scanner are shown on both the MR images and resulting 1D spectra in fig.7. These borders are also confirmed with the compartment size of 15 mm along the Z axis. Results in fig. 7 show that borders on the MR images are clearly matching with the borders on the stacked LIF spectra. It is also noted that the assignment of the Z coordinates was based on the initial registration of the device using miniature RF coil as a fiducial marker and then using the encoder reading values.

IV. DISCUSSION AND CONCLUSION

This work describes a new system and its application for robot-assisted multimodality biosensing with MRI and LIF. The system explores the area of biomedical application of

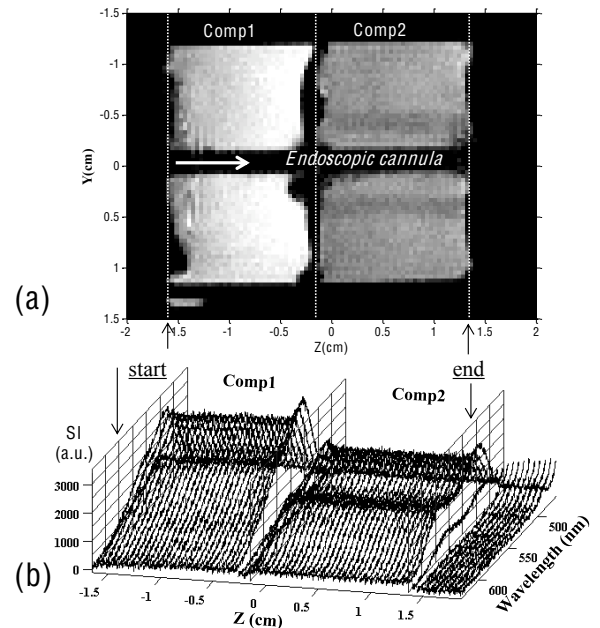


Fig. 7. (a) An MR image of the 2 compartment phantom collected with the volume RF coil. Compartments are separated by dotted lines. Scanning is performed in the “Endoscopic Cannula” and scanning direction is shown with an arrow. (b) Stack plot of LIF spectra collected with the LIF probe from the phantom shown in (a). The manipulator scanned the selected area (from “start” to the “end” as shown in the figure) every 0.5 mm along the Z direction. The spectral axis shows the wavelength in nanometers (nm). The different spectra due to different fluorophores, or non-existence of the fluorophores can be clearly visible. Compartments are separated by meshes. Each mesh corresponds to the dotted line, in the MR image.

robotic technology. Its operation principal is based on four elements: (1) the use of MRI for tissue-level imaging to identify the areas for scanning, (2) an MR-compatible computer-controlled actuated manipulator for scanning with the endoscopic LIF optical sensor (i.e. the “Limited-FOV” modality), (3) registration of this device and the LIF sensor to the MR images, and (4) generation of 1D LIF scans along the translation axis of the device and their registration to the scout images.

The core of this approach is based on registering the manipulator to the inherent coordinate system of an MR scanner by using a miniature coil as fiducial marker, this way each position of data acquisition with the Limited-FOV sensor (i.e. the LIF probe) is automatically registered to the inherent coordinate system of the MR scanner automatically.

This work, although is the first that demonstrates multi-modal MR and trans-needle optical imaging with robot-assistance, has certain experimental limitations. While such studies are suitable to demonstrate the operation of the MRI/LIF system, *in vivo* studies are needed and planned for the future. In some certain anatomies a curved access path would be more desirable; this can be a future work from our or other research groups. Additionally, although the simulation implemented in this work helped us to select the scanning resolution, additional work is underway to further improve it. First, the optical effect of prism, and quartz tubing should be considered. In this work optical fibers were simulated as directly touching to the tissue with a flat coupling. Second, this simulation is suboptimal for the vertical borders. This is since the base code [12] only simulates horizontal layers and a substantial change is needed for vertical layers.

The principle of robot-assisted multimodality imaging was introduced in [10]. As compared to this previous work, several new enabling technologies and methodologies are introduced. The most important improvement that also demonstrates the power of using robotic manipulators for multi-modal imaging and co-registration is the introduction of a novel dual MR/LIF sensor (fig. 4) for both MR and optical sensing. Minor improvements were a new actuated manipulator and the use of MR-compatible bi-directional Squiggle motors that were push-only and required a special design for bi-directional scanning.

The proposed system was designed as a generic platform for image-guided and robot-assisted scanning of the living matter. Depending on the specific needs of diagnosis or basic research, the system can carry other types of sensors, such as endoscopic OCT and CoM.

The trans-needle approach (although minimally invasive) is clinically meritorious since it allows assessment of tissue pathophysiology *in situ*. Indeed, clinically, the merit of such minimally invasive approaches can be justified if the collected information far surpasses the invasive nature of trans-needle access. This for example is the case when the

patient is a candidate for an invasive diagnostic procedure, such as tissue biopsy, as has been demonstrated before [14].

In conclusion, this work demonstrates the use of robotic methodology for multimodality sensing with MR and optical sensors that has potential impact in improving diagnosis *in situ* as well as for performing basic research *in vivo*.

REFERENCES

- [1] A. P. Smith, P. A. Hall, and D. M. Marcello, “Emerging technologies in breast cancer detection,” *Radiol Manage*, vol. 26, no. 4, pp. 16-24; quiz 25-7, Jul-Aug, 2004.
- [2] V. Ntziachristos, A. G. Yodh, M. D. Schnall *et al.*, “MRI-guided diffuse optical spectroscopy of malignant and benign breast lesions,” *Neoplasia*, vol. 4, no. 4, pp. 347-54, Jul-Aug, 2002.
- [3] S. N. Reske, N. M. Blumstein, B. Neumaier *et al.*, “Imaging prostate cancer with 11C-choline PET/CT,” *Journal of Nuclear Medicine*, vol. 47, no. 8, pp. 1249, 2006.
- [4] S. S. Kommu, R. J. Andrews, and R. W. Mah, “The future role of intelligent probes in detecting and managing prostate cancer,” *BJU international*, vol. 98, no. 4, pp. 717-719, 2006.
- [5] D. J. Margolis, J. M. Hoffman, R. J. Herfkens *et al.*, “Molecular imaging techniques in body imaging,” *Radiology*, vol. 245, no. 2, pp. 333-56, Nov, 2007.
- [6] J. Eichler, J. Knof, and H. Lenz, “Measurements on the depth of penetration of light (0.35–1.0 μm) in tissue,” *Radiation and environmental biophysics*, vol. 14, no. 3, pp. 239-242, 1977.
- [7] Q. Zhu, M. Huang, N. Chen *et al.*, “Ultrasound-guided optical tomographic imaging of malignant and benign breast lesions: initial clinical results of 19 cases,” *Neoplasia*, vol. 5, no. 5, pp. 379-88, Sep-Oct, 2003.
- [8] N. V. Tsekos, A. Khanicheh, E. Christoforou *et al.*, “Magnetic resonance-compatible robotic and mechatronics systems for image-guided interventions and rehabilitation: a review study,” *Annu Rev Biomed Eng*, vol. 9, pp. 351-87, 2007.
- [9] D. L. G. Hill, P. G. Batchelor, M. Holden *et al.*, “Medical image registration,” *Physics in Medicine and Biology*, vol. 46, pp. R1, 2001.
- [10] A. E. Sonmez, A. Ozcan, W. M. Spees *et al.*, “Robot-facilitated scanning and co-registration of multi-modal and multi-level sensing: Demonstration with magnetic resonance imaging and spectroscopy.” pp. 1133-1138.
- [11] T. S. Mang, C. McGinnis, C. Liebow *et al.*, “Fluorescence Detection of Tumors - Early Diagnosis of Microscopic Lesions in Preclinical Studies,” *Cancer*, vol. 71, no. 1, pp. 269-276, Jan 1, 1993.
- [12] L. Wang, S. L. Jacques, and L. Zheng, “MCML--Monte Carlo modeling of light transport in multi-layered tissues,” *Computer methods and programs in biomedicine*, vol. 47, no. 2, pp. 131-46, Jul, 1995.
- [13] Q. Liu, C. Zhu, and N. Ramanujam, “Experimental validation of Monte Carlo modeling of fluorescence in tissues in the UV-visible spectrum,” *Journal of Biomedical Optics*, vol. 8, no. 2, pp. 223-36, Apr, 2003.
- [14] T. D. Wang, and J. Van Dam, “Optical biopsy: a new frontier in endoscopic detection and diagnosis,” *Clinical Gastroenterology and Hepatology*, vol. 2, no. 9, pp. 744-753, 2004.